CD45R (B220; PharMingen, San Diego, CA) [HEL-biotin was prepared with biotinamidocaproate *N*-hydroxysuccinimide ester (Sigma) by standard protocols]. To detect activated lysozyme-specific Ig tg B cells, splenic MNCs were stained with HEL-biotin, followed by streptavidin-FITC and counterstained with PE-labeled anti-CD86 (B7-2) mAbs (all from PharMingen). The HEL-biotin probe stained only the adoptively transferred tg B cells, because no HEL staining was detected when B cells from DEL- or TEL-immune mice (where no adoptive transfer was performed) were stained with HEL-biotin. To confirm that the majority of the transferred tg B cells were detected with the HEL-biotin label over the 5-day period, a second labeling method was used. Splenic B cells from lysozyme-specific Ig tg mice were labeled with 2′,7′-*bis*-(2-carboxyethyl)-5-(and-6)-carboxy-fluorescein (BCECF AM) (Molecular Probes, Eugene, OR) as described (*27*) and transferred according to the adoptive transfer protocol. PBMCs and splenic MNCs of immune recipients were harvested as described above, stained with either HEL-biotin, followed by streptavidin-PE, or with biotinylated anti-CD45R (B220), followed by steptavidin-PE, and analyzed by flow cytometry. Results from three to four experiments with pooled cells from two mice demonstrated similar numbers of cells positive for both HEL binding and BCECF or B220 and BCEF.

16. Spleens were prepared for cryosections as described (*2*). For immunohistochemical staining of lysozyme-specific Ig tg B cells, a two-layer sandwich of sequential incubation with biotinylated HEL was used followed by streptavidin–alkaline phosphatase (AP), and GC B cells were detected with peanut agglutinin (PNA)–horseradish peroxidase (HRP) (EY Laboratories, San Mateo, CA). Bound HRP and AP activities were visualized by reacting with 3-aminoethyl carbazole and naphthol AS-MX phosphate–Fast Blue BB (Sigma), respectively.
17. M. C. Cook, A. Basten, B. Fazekas de St.Groth, *J. Exp. Med.* **186**, 631 (1997).
18. R. H. Carter and D. T. Fearon, *Science* **256**, 105 (1992); C. J. M. van Noesel, A. C. Lankester, R. A. W. van Lier, *Immunol. Today* **9**, 8 (1993).
19. R. C. Rickert, K. Rajewsky, J. Roes, *Nature* **376**, 352 (1995); P. Engel *et al*., *Immunity* **3**, 39 (1995).
20. On day 5 after cell transfer (as described above), 2 mg of BrdU (Sigma) was administered intraperitoneally; mice were killed 2 hours later, and spleens were analyzed by three-color immunohistochemistry (*28*). In brief, sections were blocked with Fcγ-block (1 mg/ml) (CD16/CD32, 2.4G2) and then incubated with FITC-conjugated anti-CD45R (B220, PharMingen) and HEL-biotin. After incubation with streptavidin-AP (Sigma) and anti-FITC coupled to HRP, bound HRP and AP activities were visualized as described above. Labeled sections were then treated in 1 M HCl for 20 min at 70°C to expose and partially degrade the DNA and to terminate the enzymatic reactions that had taken place previously without displacing the precipitates. Slides were then stained with mAb specific for BrdU (BU20a, Dako) and incubated with biotinylated goat anti-mouse IgG $F(ab')_2$ fragments (Boehringer) and streptavidin-AP. BrdU-positive cells were visualized with Fast Red TR/naphthol AS-MX (AP substrate: pink color).
21. R. M. Tooze, G. M. Doody, D. T. Fearon, *Immunity* **7**, 59 (1997).
22. G. G. Klaus, J. H. Humphrey, A. Kunkl, D. W. Dongworth, *Immunol. Rev.* **53**, 3 (1980); M. B. Fischer, M. Ma, N. C. Hsu, M. C. Carroll, *J. Immunol.*, in press.
23. T. Hebell, J. M. Ahearn, D. T. Fearon, *Science* **254**, 102 (1991). $[CR2]_2$-IgG1 is a fusion protein that represents the two NH_2-terminal short consensus repeats of CD21 (which includes the binding site for iC3b and C3d) coupled to the NH_2-terminus of the heavy chains of a NIP[(4-hydroxy-3 nitrophenyl)acetyl]-specific IgG1 antibody.
24. WT mice were immunized on days 1 and 7 with 50 μg of TEL as described (*12*), then received three injections (0.2 mg each, intravenously) of either sCR2 ($[CR2]_2$-IgG_1) ($n = 4$) (*23*) or control IgG_1 ($n = 5$) on days 10, 11, and 12. After 48 hours, spleens were harvested, quick-frozen in OCT, and examined by immunohistological staining (B220, blue; PNA, crimson) as described (*16*). Results show significant reduction in both the mean number of PNA^+ GCs and the GC area of sCR2-treated animals. Total GC area per spleen (mean GCs per spleen × mean area per GC = mean GC area per spleen) was determined by morphometric analysis of at least three sections per spleen of animals injected with either sCR2 ($n = 4$) or control IgG1 ($n = 5$). sCR2 versus control mAb (mean ± SEM, Student's *t* test): GCs per spleen = 9.5 ± 1.6 versus 34.0 ± 2.8 ($P < 0.4 \times 10^{-6}$); area per GC = 11.20 ± 1.29 versus 24.67 ± 1.75 μm^2 ($P < 0.2 \times 10^{-6}$); total GC area per spleen = 106.40 versus 837.78 mm^2.
25. J. Wu *et al*., *J. Immunol.* **157**, 3404 (1996); D. Qin, J. Wu, M. C. Carroll, G. F. Burton, A. K. Szakal, J. G. Tew, in preparation.
26. E. M. Prager and A. C. Wilson, *J. Biol. Chem.* **246**, 5978 (1971).
27. T. G. Diacovo, K. D. Puri, R. A. Warnock, T. A. Springer, U. H. von Andrian, *Science* **273**, 252 (1996).
28. B. Zheng, S. Han, G. Kelsoe, *J. Exp. Med.* **184**, 1 (1996).

29. We thank M. Gendelman for preparation of the antibody to sCR2 and control antibody and E. Alicot for assistance with the analyses of sCR2-treated mice; J. Cohen (Harvard Medical School) for NH_2-terminal amino acid sequence analysis; and D. T. Fearon (Cambridge, UK) and T-Cell Sciences (Boston, MA) for the $[Cr2]_2$-IgG1 hybridoma. Supported by the Austrian Science Foundation (M.B.F.), DAAD Sonderprogramm Rheumatologie, Germany (S.G.), the National Institutes of Health (M.C.C. and G.K.), and the New York Chapter of the Lupus Foundation (M.C.C.).

17 November 1997; accepted 18 February 1998

Visualization of Single RNA Transcripts in Situ

Andrea M. Femino, Fredric S. Fay,† Kevin Fogarty, Robert H. Singer*

Fluorescence in situ hybridization (FISH) and digital imaging microscopy were modified to allow detection of single RNA molecules. Oligodeoxynucleotide probes were synthesized with five fluorochromes per molecule, and the light emitted by a single probe was calibrated. Points of light in exhaustively deconvolved images of hybridized cells gave fluorescent intensities and distances between probes consistent with single messenger RNA molecules. Analysis of β-actin transcription sites after serum induction revealed synchronous and cyclical transcription from single genes. The rates of transcription initiation and termination and messenger RNA processing could be determined by positioning probes along the transcription unit. This approach extends the power of FISH to yield quantitative molecular information on a single cell.

The identification of specific nucleic acid sequences by FISH has revealed sites of RNA processing, transport, and cytoplasmic localization (*1*). Recognition of these sites of hybridization is possible only when sufficient concentrations of the target sequence provide contrast with regions of lesser or no signal. Here we describe a quantitative approach to identify single molecules in these regions of low concentration. The methodology also facilitates accurate quantitation of the regions containing multiple copies of RNA, such as is found at transcription sites. Analysis of individual transcription sites with single molecule accuracy generated precise information on nascent chain initiation, elongation, and termination.

FISH images are composed of points of light with variable intensities resulting either from hybridization or from background fluorescent noise. We used multiple probes targeted specifically to β-actin mRNA to generate high-intensity point sources that result from hybridization to individual RNAs. We then quantitated the light intensity from each point source to distinguish hybridization events from spurious fluorescence.

The strategy involves (i) synthesizing several oligonucleotide probes to adjacent sequences on an RNA target such that their collective fluorescence will be emitted as a point source after hybridization; (ii) conjugating fluorochromes to specific sites on each oligonucleotide probe so that the fluorescent output per molecule of probe can be calibrated (Fig. 1, A to C); (iii) acquiring digital images from a series of focal planes through a hybridized cell; and (iv) processing these images with a constrained deconvolution algorithm such that out-of-focus light is quantitatively restored to its original points of origin.

To identify single β-actin mRNA molecules, we hybridized multiple probes to the isoform-specific 3′-untranslated region (UTR) of the mRNA in normal rat kidney (NRK) cells. The acquired fluorescence image was made up of numerous bright points

A. M. Femino and R. H. Singer, Department of Anatomy and Structural Biology and Cell Biology, Albert Einstein College of Medicine, Bronx, NY 10461, USA.
F. S. Fay and K. Fogarty, Biomedical Imaging Facility and Department of Physiology, University of Massachusetts Medical School, Worcester, MA 01655, USA.

*To whom correspondence should be addressed.
†Deceased.

of fluorescence interspersed within a diffuse, lower intensity signal (Fig. 1D). After deconvolution, the image consisted of numerous distinct points of light throughout the cytoplasm (Fig. 1E). The brightest points of light were constrained to a few contiguous volume elements (voxels). The image also contained scattered single voxels and clusters of voxels with low amounts of fluorescent signal attributed to low-level autofluorescence and sources of background noise. Establishing an image threshold removed ~95% of these voxels (Fig. 1, F and G). The discrete, brightest clusters that remained after a threshold was established are referred to as objects. The total fluorescence intensity (TFI) of each object was then calculated. These bright objects had TFI values expected for single molecules and fell within the range of one to five probes hybridized (Fig. 1H). This analysis supports the conclusion that single molecules of β-actin mRNA were being detected and that they corresponded to the points of light. The β-actin mRNA molecules were often far enough apart to be resolved by light microscopy as individual point sources.

Additional evidence that these points of light are single molecules comes from an analysis of their prevalence. A population of cells grown in serum-free medium contained 500 ± 200 β-actin mRNAs per cell. In an exponentially growing population of cells the number increased to ~1500 copies, consistent with activation of actin mRNA transcription and possible stabilization of cytoplasmic actin mRNA by serum (*2*, *3*). This copy number of β-actin mRNA agrees with estimates of the average abundance of β-actin mRNA per cell derived from molecular techniques (*4*).

Finally, spectrally distinct probes hybridized to different target sequences on the same mRNA molecule were used to verify single molecule detection. When the probes were targeted to the same molecule, the signals were close together (Fig. 2C). The TFI confirmed that they were hybridized to only one molecule. Statistical analysis of 478 signals in the cell determined that 59% of the red signals were ≤3 voxels (279 nm) from a green signal. As a control, two isoforms of actin mRNA, β and γ, were detected simultaneously in the same cell with probes that were specific for each isoform (Fig. 2, A and B). The gene sites for each isoform were distinguishable in the nucleus

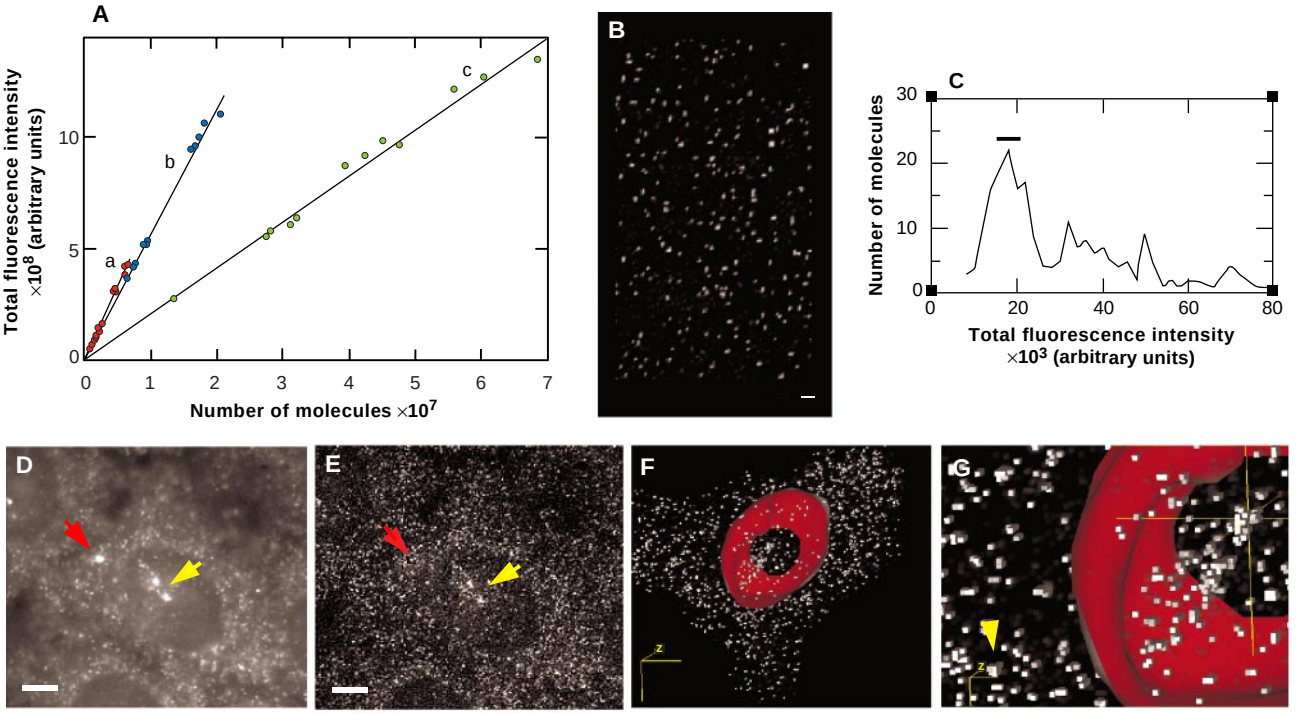

Fig. 1. Methodology for detection of single RNA molecules by quantitative FISH and digital imaging microscopy (*13*). Probes used are described in (*14*). (**A**) The amount of light emitted per probe was calibrated by measuring the TFI from a known number of probes in an imaged volume (*15*). The TFI was plotted against the number of fluorochrome molecules (five per probe) to generate the regression curve. The slope is equal to the TFI per fluorochrome (curve a = CY3, curve b = CY5, curve c = FITC). A normalized TFI per probe was used to calculate the number of probes hybridized at discrete point sources of light in a restored image (*15*). (**B**) The accuracy of the technique was tested by optically sectioning and restoring immobilized CY3-labeled probes adsorbed to glass cover slips. (**C**) The most frequent occurrences of TFI values per CY3 probe plotted as a histogram are comparable to the normalized value (solid bar) from the solution experiments (*16*). (**D**) One optical plane of an NRK cell after in situ hybridization (*17*) with calibrated CY3 probes to β-actin mRNA shows a number of bright foci superimposed on a diffuse background arising from out-of-focus light. Red arrow, bead = 0.099 μm; yellow arrow, two transcription sites. (**E**) The fluorescent probe distribution after image restoration with an iterative constrained algorithm, EPR (*18*). The restored image reveals discrete points of light, which allow accurate measurement of the TFI emanating from each point source (bead is restored to a point source). The image is a two-dimensional (2D) projection of the 3D restored image. (**F**) The thresholded image (*19*) is rendered so that the cell is viewed from the bottom looking upward into the nucleus (*20*). The red surface portrays the boundary of the nuclear envelope. The opening in the center of the nuclear surface is a result of truncating the upper optical sections. (**G**) Enlargement of (F) showing the dimensions of a restored transcription site in the nucleus (cross hairs), in contrast to a 100-nm bead (yellow arrow), the most intense object in the image, restored to a point source (*21*). (**H**) The integrated TFI value of each point was mapped to a single voxel and the number of probes hybridized assigned a color and frequency [1 = violet, 25.2%; 2 = blue, 33.6%; 3 = green, 17.5%; 4 = yellow, 11.6%; 5 = orange, 6.8%; >5 = red, >10 = white, <5%; *n* = 681 molecules per cell, 95% efficiency of hybridization was estimated from a binomial distribution (*22*)] (*23*). In (D) to (F), scale bar = 5 μm; in (B) and (G), scale bar = 1 μm.

and the mRNAs as separate point sources in the cytoplasm. In contrast to the cis probes, the signals did not colocalize significantly; they were ≤3 voxels apart 13% of the time.

Visualization and measurement of intramolecular distances were possible when the cis probes were sufficiently separated (Fig. 2, C and D). To ascertain that the displacement of the hybridization signal was not an artifact due to misalignment of the respective red and green images, we hybridized three probes, each labeled with distinct fluorochromes, to β-actin mRNA at distances of 1648 nucleotides (nt) (maximum) and 631 nt (minimum) apart. We found that the registered images from the maximally distant probes were not coincident (as much as 487 nm apart), whereas near probes were within the same voxel. This result indicated that the detected mRNA was almost completely extended (1648 kb × 0.3 nm per nucleotide = 494 nm).

To verify that a single copy sequence could be detected by this method, we hybridized 10 probes, each with six CY3 fluorochromes, to the template strand of the β-actin gene (Fig. 3A). Eleven probes, each with five fluorescein isothiocyanate (FITC) fluorochromes, targeted to the β-actin nascent transcripts were used simultaneously (Fig. 3B) and verified the gene site by colocalization (Fig. 3C). The TFI values obtained for hybridization to the single DNA target (60 fluorochromes) were consistent with the TFI predicted from single mRNAs. The nascent transcripts gave a much brighter signal than the gene because they represented multiple RNA molecules concentrated at that site. Measurement of 130 genes revealed the distribution of fluorescence expected from the independent hybridization of 10 probes (Fig. 3D). The hybridization efficiency was close to 100%, because all 10 probes hybridized most frequently. Hybridization to nascent transcripts indicated the presence of multiple copies corresponding to a maximum of 68 probes per transcription site.

This technology allowed us to quantitate the kinetics of β-actin mRNA transcription (Fig. 4). Cells cultured overnight in serum-free medium showed essentially no detectable transcriptional activity (Fig. 4A). The addition of serum (*2*) resulted in synchronous activation of transcription detected on one of the β-actin alleles in virtually every cell within a few minutes (Fig. 4B). The number of nascent transcripts per β-actin allele was determined with a single probe to the 5′-UTR. The simultaneous use of 3′-UTR probes provided information on the number of polymerase molecules that had progressed to the terminal portion of the gene. At 3 min after induction, the average gene contained 12 nascent RNAs, but few 3′-UTR signals (Fig. 4, B and G). By 4 min, both β-actin alleles were transcriptionally active in almost all cells, and four transcripts had entered into the 3′-UTR (Fig.

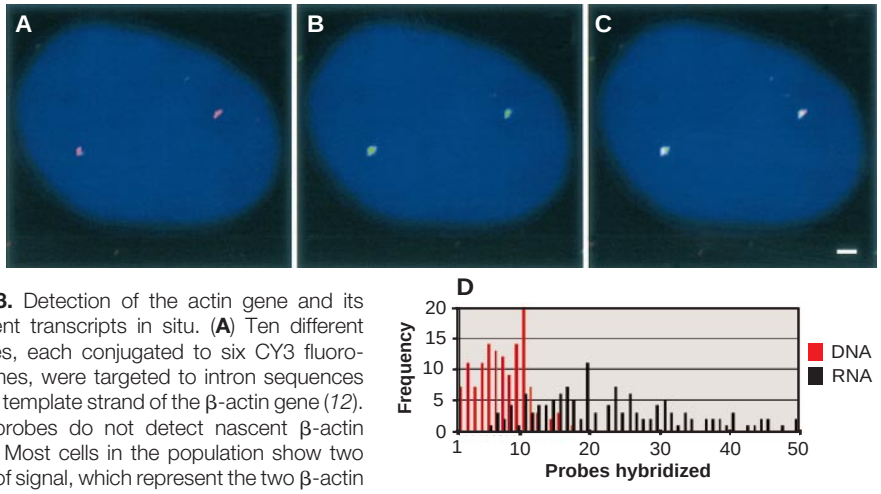

Fig. 3. Detection of the actin gene and its nascent transcripts in situ. (**A**) Ten different probes, each conjugated to six CY3 fluorochromes, were targeted to intron sequences of the template strand of the β-actin gene (*12*). The probes do not detect nascent β-actin RNA. Most cells in the population show two sites of signal, which represent the two β-actin alleles. (**B**) Different unique probes, each labeled with five FITC fluorochromes, were targeted to the 5′-UTR (one probe), splice junctions (five probes), and 3′-UTR (five probes) for β-actin RNA. Represented here are two sites of intense signal in the nucleus, indicating sites of active transcription in response to serum stimulation. (**C**) Both signals, detecting the DNA and nascent RNA, respectively, colocalize upon superimposition. (**D**) A frequency histogram shows an abrupt truncation at the TFI for the 10 fluorescent probes hybridized to DNA, indicating the detection of a single copy of the β-actin gene. The histogram for nascent RNA shows a broad profile of hybridization, indicating multiple copies at each gene site (truncated at 50). Bar = 1 μm.

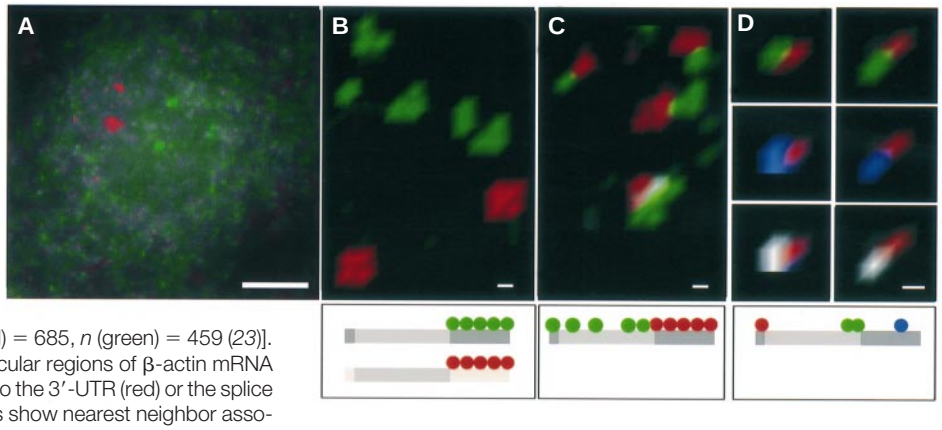

Fig. 2. Probing of intermolecular and intramolecular targets in the cytoplasm. (**A**) The detection of trans sequences. Both β- (green) and γ- (red) actin mRNA were detected simultaneously in the same cell with probes to their respective 3′-UTRs. The transcription sites for each isoform were visible in the nucleus. (**B**) Individual β- and γ-actin mRNAs segregate independently in the cytoplasm [statistical analysis of the frequency of measured separation distances in voxels (vo) (1 vo = 93 nm by 93 nm by 100 nm) between red and the nearest green signal is expressed as cumulative percent: 0 vo = 0.1%, 1 vo = 1.5%, 2 vo = 6.4%, 3 vo = 13.7%, 4 vo = 25.1%, 5 vo = 36.5%; *n* (red) = 685, *n* (green) = 459 (*23*)]. (**C**) The detection of *cis*-sequences. Two intramolecular regions of β-actin mRNA are resolved with five different probes (*12*) targeted to the 3′-UTR (red) or the splice junction (SJ) sites (green). β-Actin mRNA molecules show nearest neighbor association of the 3′-UTR and the coding region. Frequency of separation distances in voxels: 0 vo = 2.4%, 1 vo = 15.8%, 2 vo = 32.9%, 3 vo = 59.1%, 4 vo = 72.6%, 5 vo = 87.2%; *n* (red) = 164, *n* (green) = 314. The 3′-UTR probes (red) are used to specifically detect β-actin mRNA. The SJ probes for β-actin (green) have homology with γ-actin, accounting for more green than red signal (*23*). Respective red and green pairs had TFI values consistent with single β-actin mRNA molecules. (**D**) Intramolecular measurement with three spectrally distinct probes hybridized to two β-actin mRNAs. Two regions 631 bases (190 nm) apart were not resolved (CY5, blue; FITC, green); a third region, 1648 bases away (500 nm), was resolved (CY3, red). The colocalized voxels of the blue and green images are turned white. The distance between red and blue maxima is estimated to be 487 nm, consistent with a linear RNA. The schematic depicts the locations of the probes. In (A), bar = 5 μm; in (B) and (C), bar = 93 nm; and in (D), bar = 187 nm.

4G). These results are consistent with a transcription rate of 1.1 to 1.4 kb/min (5). The mean number of nascent transcripts associated with each gene increased linearly from 0 to 5 min, with a mean increase of four transcripts per minute (Fig. 4H). Few transcripts dissociated from the site during this 5-min interval, as evidenced by the probe fluorescence constrained to the location of the gene (Fig. 4C).

Between 5 and 15 min after induction, the number of nascent RNA transcripts per allele increased steadily and peaked at 15 min, with an average of 30 nascent transcripts per allele (Fig. 4H). During the same period, the mean number of transcripts traversing the 3′-UTR reached a steady-state value of 8 to 10, indicating that the rate of entry of new transcripts into this region was equal to the rate of transcripts terminating. At this time, spots of fluorescence were detected around the transcription site (Fig. 4, D and E). These point sources of fluorescence were less intense than the transcription sites. Their TFI values were identical to the points of signal in the cytoplasm; therefore, we interpreted them to be single, terminated transcripts leaving the site of the gene.

Because the released transcripts did not accumulate significantly in the immediate vicinity of the gene after the expected time of termination, we concluded that the initiation of transport took no more than a few minutes. The dispersal of transcripts away from the transcription site took on a variety of spatial patterns (Fig. 4, D and E). Often tracklike distributions were apparent, and the regular spacing between points suggested a constant rate of movement away from the transcription site. Occasionally, the transcripts appeared to spiral away from the site of transcription; however, in at least half of the cases examined, the terminated transcripts simply appeared to diffuse around the site, without any discernible pattern. Nascent transcripts diminished at 60 min after serum induction (Fig. 4F). The decline of transcriptional activity beginning at 30 min fit an exponential decay profile for the next 1.5 hours, at which time it became indistinguishable from the state before induction (Fig. 4H). Over the induction period beginning at 10 min, there was a constant increase in the number of single β-actin mRNA molecules in the cytoplasm (6).

The capacity of these procedures to generate accurate information about single cells was illustrated by a high-resolution, dynamic view of each β-actin mRNA transcription site obtained with three probes positioned along the RNA, each labeled with a different fluorochrome (Fig. 4I). A "snapshot" of a representative gene revealed 23 nascent RNAs in the process of elongation, 14 of which had progressed through the proximal 3′-UTR and 8 of those through the distal 3′-UTR. At least five of the RNAs had passed the cleavage and polyadenylation site. These RNAs may be nascent, cleaved but undergoing polyadenylation, or awaiting transport. These possibilities should be distinguished by using probes downstream from the cleavage and polyadenylation site. The rat β-actin gene has a consensus "termination" sequence at the predicted distance downstream of the polyadenylation sequence that might account for this observation (7). The average spacing between polymerases in the 3′-UTR was ~60 nt, whereas in the 5′-region of the gene, it was ~170 nt. This spacing is consistent with previous observations on polymerase II (Pol II) transcription loading (8). The closer packing of polymerases in the 3′-UTR of the gene suggest-

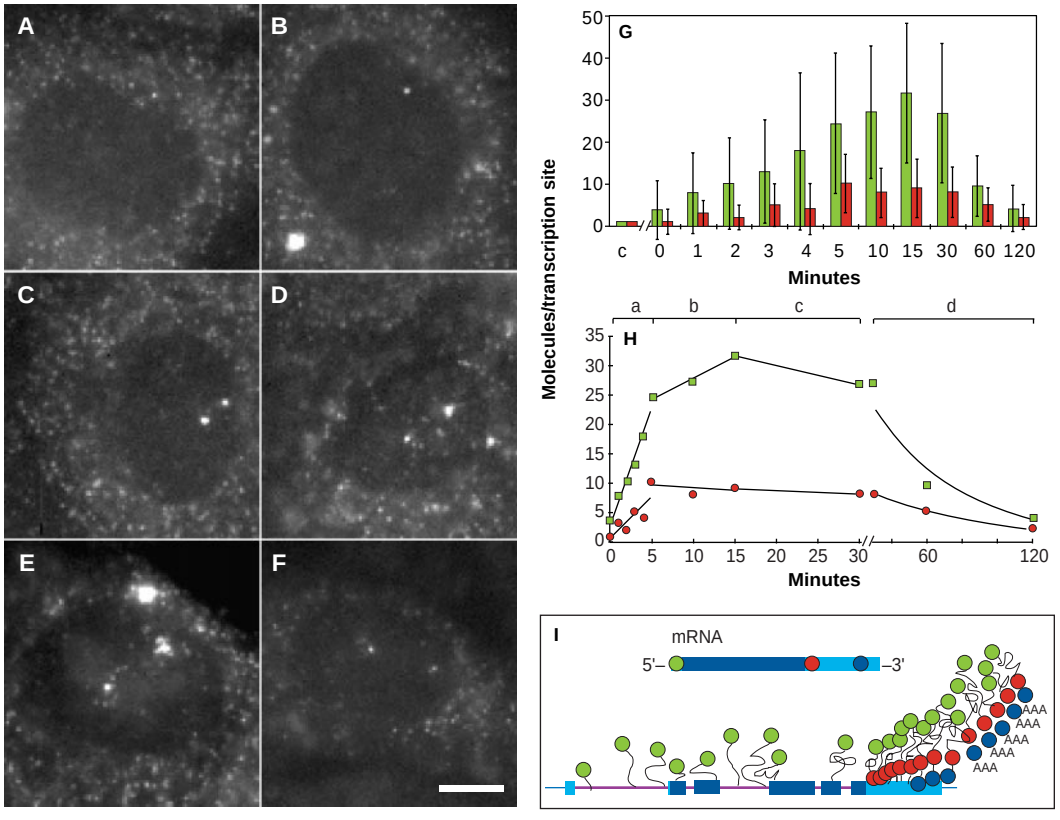

Fig. 4. The kinetics of serum induction and subsequent transcription of the β-actin gene. (**A** to **F**) Images captured the progression of transcription into the 3′-UTR from quiescence at 0 min (A), one site active at 3 min (B), both sites at 5 min (C), peak of transcriptional activity and RNA export at 10 min (D) and 15 min (E), to a decline at 60 min (F). (**G**) Quantitative analysis of the transcription sites. The histogram indicates the mean number of nascent RNA on the gene (green) in the cell population at various times after induction and the mean number of nascent RNA that entered the 3′-UTR (red). The error bars indicate variation in transcriptional activity between the β-actin alleles in the same cell as well as within the cell population. The signal from the 5′ and 3′ end of one mature mRNA is represented as a scale (c). (**H**) Separate regression curves were fitted to the following intervals: (section a) 0 to 5 min, before termination; (section b) 5 to 15 min, transcripts were terminating while the total number of transcripts on the gene continued to increase, and the number of RNAs in the 3′-UTR reached a plateau; (section c) 15 to 30 min, a slow decline in the total number of nascent RNA with little change in the number located in the 3′-UTR; and (section d) 30 to 120 min, an exponential decline in the total number of nascent RNA and in RNA reaching the 3′-UTR. (**I**) A dynamic profile of transcription at one β-actin allele resolved with three spectrally distinct probes (*14*). The 5′-UTR probe detects all the nascent RNA (green). A second probe detects RNA that has progressed beyond the first 50 bases of the 3′-UTR (red), and the third probe detects RNA that has progressed to the distal region of the 3′-UTR (blue). The triple A's indicate transcripts beyond the polyadenylation site. Bar = 5 μm.

ed that termination and release were rate limiting. Recent work indicates that Pol II recruits cleavage and polyadenylation factors, which may result in the polymerase slowing at this point (*9*).

The rate of increase (four transcripts per minute) in the number of nascent transcripts from 0 to 5 min reflects solely the rate of initiation, because few polymerases should have reached the termination site, on the basis of the rate of elongation. An in vitro system indicated that Pol II can initiate at a rate of two transcripts per minute (*10*). Between 5 and 15 min, when termination was occurring, there was a sustained increase of one nascent RNA per minute. Assuming that the initiation rate remained constant, then the rate of termination and release would be three RNA per minute. Surprisingly, there was a precipitous decrease of activity at the transcription site after 30 min. The cycle of the transcriptional pulse in response to serum is similar to that shown for c-*fos* (*11*). By interrogating the site with probes along the length of the RNA, we determined that this shut-down resulted from an inhibition of initiation rather than "pausing" of the polymerases. There was no apparent accumulation of transcripts at the nuclear envelope, so it is likely that export is not rate limiting.

The advance herein evaluates FISH images so that single molecule signals are not eliminated through background subtraction or the establishment of a threshold. As a consequence of this approach, single mRNA molecules were detectable with as little as one oligonucleotide probe, containing only five fluorochromes, an increase in sensitivity more than two orders of magnitude greater than previously obtained (*12*). In addition, the template DNA strand was accessible to the small probes during transcription without denaturation, contrary to other protocols, and may indicate that it contained single-stranded regions. This technique may therefore allow probing of the active regions of chromatin and facilitate detection of specific genes or groups of genes where only short, nonrepetitive sequences can be used. This would bring many physiologically important genes for receptors, signaling molecules, cell cycle regulators, and transcription factors, as well as their nuclear and cytoplasmic transcripts, into range of FISH detection.

REFERENCES AND NOTES

1. J. B. Lawrence, R. H. Singer, L. M. Marselle, *Cell* **57**, 493 (1989); C. L. Sundell and R. H. Singer, *Science* **253**, 1275 (1991); G. Zhang, K. L. Taneja, R. H. Singer, M. R. Green, *Nature* **372**, 809 (1994); R. M. Long *et al*., *Science* **277**, 383 (1997).
2. P. K. Elder, L. J. Schmidt, T. Ono, M. J. Getz, *Proc. Natl. Acad. Sci. U.S.A.* **81**, 7476 (1984).
3. M. E. Greenberg, A. L. Hermanowski, E. B. Ziff, *Mol. Cell. Biol.* **6**, 1050 (1986).
4. J. B. Lawrence and R. H. Singer, *Nucleic Acids Res.* **13**, 1777 (1985); R. J. Schwartz and K. N. Rothblum, *Biochemistry* **20**, 412 (1981).
5. C. S. Thummel, *Science* **255**, 39 (1992); A. W. Shermoen and P. Z. O'Farrell, *Cell* **67**, 303 (1991).
6. A. M. Femino, F. S. Fay, K. Fogarty, R. H. Singer, data not shown.
7. R. Ashfield *et al., EMBO J.* **13**, 5656 (1994); R. Ashfield, P. Enriquez-Harris, N. Proudfoot, *ibid.* **10**, 4197 (1991).
8. Y. N. Osheim, O. L. Miller, Jr., A. L. Beyer, *Cell* **43**, 143 (1985).
9. J.-C. Dantonel, K. G. K. Murthy, J. M. Manley, L. Tora, *Nature* **389**, 399 (1997).
10. D. K. Hawley and R. G. Roeder, *J. Biol. Chem.* **262**, 3452 (1987).
11. S. Huang and D. L. Spector, *Genes Dev.* **5**, 2288 (1991).
12. R. W. Dirks, K. C. Daniel, A. K. Raap, *J. Cell Sci.* **108**, 2565 (1995); Y. Xing, C. V. Johnson, P. T. Moen Jr., J. A. McNeil, J. Lawrence, *J. Cell. Biol.* **131**, 1635 (1995).
13. For details of the digital imaging microscopy procedures, see F. S. Fay, K. E. Fogarty, J. M. Coggins, *Soc. Gen. Physiol. Ser.* **40**, 51 (1986); F. S. Fay, W. A. Carrington, K. E. Fogarty, *J. Microsc.* **153**, 133 (1989). Images were obtained with an inverted Nikon Diaphot 200 epifluorescence microscope equipped with a 100-W mercury lamp and modified to capture images under computer control. Between 20 to 35 optical sections were acquired at 250-nm z-intervals and at an effective pixel size of 187 nm by 187 nm with a thermoelectrically cooled (–45.0°C) charge-coupled device (CCD) (model 220; back-thinned RCA CCD chip; 50 kHz; Photometrics, Tucson, AZ). A high quantum efficiency (0.8 at 500 nm) and a low noise (50 photons equivalent) were required for imaging at the low light levels.
14. Oligonucleotide probes were synthesized, purified, and labeled as described [E. H. Kislauskis, Z. Li, R. H. Singer, K. L. Taneja, *J. Cell Biol*. **123**, 165 (1993)] (*23*). Below are listed the probes used in this work (nucleotide number start, length in nucleotides). The sequence is for β-actin unless specified (accession J00691). For Fig. 1, B and D through H, the antisense probes to the 3′-UTR were 3133, 51; 3312, 52; 3434, 53; 3488, 52; and 3542, 52. For Fig. 2, same as Fig. 1 and the antisense probes to the γ-actin (accession X52815) 3′-UTR were 1151, 50; 1282, 61; 1409, 52; 1470, 54; and 1535, 56. For Fig. 2C, same as Fig. 1 and the antisense probes to the splice junctions were (exon nucleotides only) 284, 52; 1340, 52; 1667, 52; 2567, 56; and 2839, 53. For Fig. 2D, the antisense probe to the 5′-UTR was 255, 50; to the coding region, 2839, 53 and 3034, 52; and to the 3′-UTR, 3542, 52. For Fig. 3A, the sense probes to the introns were 630, 63; 998, 63; 1069, 63; 1369, 63; 1691, 61; 1889, 64; 1960, 63; 2040, 63; 2590, 63; and 2864, 62. For Fig. 3B the antisense probe to the 5′-UTR was 225, 53; to the splice junctions, the same as Fig. 2; and to the 3′-UTR, the same as Fig. 1. For Fig. 4, A through F, the antisense probe to the 5′-UTR was 225, 53 and the antisense probes to the 3′-UTR were 3133, 51; 3312, 52; 3434, 53; 3488, 52; and 3542, 52. For Fig. 4I, the antisense probe to the 5′-UTR was 255, 50, and the antisense probes to the 3′-UTR were 3133, 51 and 3542, 52.
15. The TFI per probe was measured by using a known concentration of fluorochrome in a determined volume between a cover slip and slide as follows: (i) Probes were dispersed in a solution equivalent in composition to mounting medium with final concentrations ranging from 0.25 to 4.0 ng/μl for cyanine (CY)3- and CY5-labeled probes and 1.0 to 16 ng/μl for FITC-labeled probes. (ii) Fluorescent beads (200 nm in diameter) adhered to the glass surfaces and delineated the distance between the inner surfaces of the cover slip and slide when brought into focus at each surface. The stage position was monitored with an Eddy-current sensor and was used to measure the vertical distance between the two beads to determine the height of the volume element containing the probe solution. (iii) A single plane in the middle was imaged and contained the total fluorescence contributed by all the fluorescent molecules in solution above and below the plane of focus in the imaged volume [imaged volume = $(x)(y)(z)$ μm^3]. The pixel size was calibrated for the optical setup of the microscope ($x = y$ = 93 or 187 nm with a ×60 magnification, 1.4 numerical aperture objective, and ×5 or ×2.5 camera eyepiece, respectively). The TFI is dependent on the light flux at the sample; therefore, a calibration curve was calculated for each imaging session. The slope is equal to the TFI per fluorochrome under imaging conditions (CY3: $m = 65 \pm 1.3$, $R = 0.992$; FITC: $m = 20.6 \pm 0.8$, $R = 0.985$; CY5: $m = 56.3 \pm 1.4$; correlation coefficient $R = 0.992$). Exposure times for CY3, FITC, and CY5 were 3, 4, and 15 s, respectively. (iv) The TFI value per probe obtained from solution was adjusted to that for a restored image and multiplied by a factor (50) equal to the number of optical sections in the point spread function (PSF) used for deconvolution of the experimental image. The TFI for one probe molecule is calculated and normalized to that for a restored image (CY3, 16250 ± 975; FITC, 5150 ± 600; and CY5, 14075 ± 1050). For exhaustive photon reassignment (EPR), the sampled PSF defines the depth (number of optical sections) over which light is integrated by the deconvolution process.
16. Fluorescent probes diluted in mounting media (2 pg/μl) were allowed to adsorb to the surface of a cover slip and then optically sectioned. The restored images revealed the distribution of intensities attributed to individual probes. The empirical measurements of the TFI for one probe either in solution or immobilized on glass cover slips were compared with a theoretical estimate of the number of photons emitted by one dye molecule by using the molar extinction coefficient, the quantum yield, the measured light flux of the microscope, and the quantum efficiency of the CCD camera. This estimate came within 80% of the actual measurement obtained.
17. For cell culture and in situ hybridization, NRK cells (djf clone from parent cell line, NRK-52E, American Type Culture Collection CRL 1571) were grown to confluence on 22 mm by 22 mm acid-washed cover slips in F12K media supplemented with 10% fetal bovine serum (FBS). The djf clone showed serum-responsive β- and γ-actin genes. For serum induction experiments, cells were incubated with F12K media (0.5% FBS) for 24 hours and then stimulated with 10% FBS. Cells were fixed for 10 min at room temperature in 4% paraformaldehyde in phosphate-buffered saline (PBS) (2.7 mM KCl, 1.5 mM KH_2PO_4, 137 mM NaCl, 8 mM Na_2HPO_4) after serum stimulation, washed, and stored in PBS. The FISH protocol was modified from K. L. Taneja and R. H. Singer [*J. Cell. Biochem.* **44**, 241 (1990)]. Cells were hybridized for 3.5 hours at 37°C. Cover slips were washed and mounted on slides with phenylenediamine in 90% glycerol with PBS. Multicolored (FITC, tetramethyl rhodamine isothiocyanate), 0.099-μm-diameter latex beads (Molecular Probes) were included in the mounting media and used as fiduciary markers to align images.
18. To elucidate the true fluorescence distribution of the acquired image, we restored the series of optical sections by using an iterative algorithm (Exhaustive Photon Reassignment, EPR) that used non-negativity constraints. Images were restored with 400 iterations and a smoothing factor alpha value = 5×10^{-6} and a convergence value of 0.001. The procedure has been detailed previously [W. A. Carrington *et al.*, *Science* **268**, 1483 (1995); K. L. Taneja, L. M. Lifshitz, F. S. Fay, R. H. Singer, *J. Cell Biol*. **119**, 1245 (1992)].
19. Background in a restored image comprises point sources of low-level autofluorescence, light scattering, and random noise contributed by the imaging electronics. A threshold value was established and applied to the restored images to eliminate these low-level point sources of light by analyzing the background TFI frequency distribution of nonzero pixels in a cell subjected to a mock hybridization. The mean TFI per nonzero voxel +3 SD was chosen as the threshold value; all pixels less than the threshold value were set to zero, whereas those greater were

retained at their original value. This eliminated >95% of the low-TFI background pixels. The threshold value was <10% of that predicted for one probe molecule (five CY3 fluorochromes) and when applied to the experimental image did not adversely affect the value from one hybridized probe. Brighter background pixels that eluded the thresholding filter but whose TFI value was less than that for one hybridized probe were excluded during the mapping analysis. The result was a filtered image where one hybridized CY3 labeled probe could be distinguished.
20. Data Analysis and Visualization Environment (DAVE); copyright 1995 by Lawrence M. Lifshitz and the University of Massachusetts Medical School.
21. The reassignment of light to a point source in a restoration results in one or two brighter voxels at the location of the point source in addition to a number of associated contiguous voxels. A point source is thus described as an object comprising a group of contiguous nonzero voxels in a restored image after thresholding. All the nuclear and cytoplasmic point sources therefore had a finite size and were treated as three-dimensional objects.
22. Additional evidence that every discrete signal is a single RNA molecule is that, when each of the five probes was hybridized individually, analysis showed that >95% of the detected sites had one probe hybridized. When two probes to the 3′-UTR were used, a population of single and double probes was detected (*6*). As an additional control, a set of five probes to an mRNA not expressed in these cells (α-actin) gave about 20 single probe signals per cell (2% of the β-actin single probe signal), but no multiple probe signals when processed by identical methods.
23. Supplementary material is available at www.sciencemag.org/feature/data/975399.shl. General information is available at www.singerlab.aecom.yu.edu.
24. We thank members of the Biomedical Imaging Facility, L. M. Lifshitz and J. Collins for their assistance with the DAVE software, R. A. Tuft for carrying out the light-flux measurements of the microscope, Y.-L. Wang for NRK cells, and K. Taneja for oligonucleotide probe synthesis. Supported by NIH grant GM 54887 to R.H.S. We are deeply saddened by the loss of our colleague and close friend Fredric S. Fay during the preparation of this manuscript.

3 October 1997; accepted 20 February 1998

In Situ Visualization of DNA Double-Strand Break Repair in Human Fibroblasts

Benjamin E. Nelms,* Richard S. Maser,* James F. MacKay, Max G. Lagally, John H. J. Petrini†

A method was developed to examine DNA repair within the intact cell. Ultrasoft x-rays were used to induce DNA double-strand breaks (DSBs) in defined subnuclear volumes of human fibroblasts and DNA repair was visualized at those sites. The DSBs remained in a fixed position during the initial stages of DNA repair, and the DSB repair protein hMre11 migrated to the sites of damage within 30 minutes. In contrast, hRad51, a human RecA homolog, did not localize at sites of DNA damage, a finding consistent with the distinct roles of these proteins in DNA repair.

Proteins that mediate certain aspects of DNA metabolism, such as DNA replication, appear to be compartmentalized within the nucleus. DNA replication therefore requires the movement of DNA to and from established sites within the nuclear matrix (*1*). Cytologic analyses have revealed that the DSB repair proteins hRad51 and the hMre11-hRad50 complex assemble in discrete nuclear foci as part of the normal cellular response to DNA damage (*2*–*5*). These findings may indicate that DNA repair does not entail the movement of DNA DSBs to preexisting intranuclear sites. Rather, they suggest that DNA repair proteins move to sites of DNA damage. The inability to detect DSBs in situ has made it difficult to address this issue experimentally. A method to induce and subsequently detect DSBs within a defined subnuclear volume would, in principle, provide a means to determine whether DSB repair requires the movement of DNA repair proteins to the sites of DNA damage.

To that end, we developed a method to examine the temporal and spatial nature of DSB repair within the context of the intact cell. This method relies on synchrotron-generated ultrasoft x-rays [<5000 electron volts (5 keV)], a multilayer monochromator for tunable ultrasoft x-ray energies with sufficient intensity for irradiation of live human fibroblasts (*6*), and microfabricated irradiation masks to induce DNA damage in discrete subnuclear regions of irradiated cells (Fig. 1) (*7*). The irradiation masks were fabricated with x-ray lithography and consist of gold stripes (1.85 μm wide with 1.35-μm separation) deposited on thin Si_2N_4 membranes (*7*). Dosimetric analyses with the irradiation mask showed that gold-shielded regions receive about 0.5% of the dose absorbed by the nonshielded regions (*7*). Irradiated cells thus absorb ultrasoft x-rays in 1.35-μm-wide stripes separated by 1.85-μm gaps that remain essentially unirradiated.

The 1.34-keV ultrasoft x-rays used in these experiments act almost exclusively through photoelectric interactions in biological material (*8*), resulting in low-energy electrons that have very short track lengths (<50 nm), comparable to the dimensions of biologically relevant structures such as chromatin (*9*). These properties suggested that photoelectrons and Auger electrons as well as free radicals resulting from absorption of ultrasoft x-rays would induce DNA damage almost exclusively within the 1.35-μm stripes imposed by the grids. Human fibroblasts (37Lu) were irradiated and DSBs were labeled with bromodeoxyuridine triphosphate (BrdU) and terminal deoxynucleotidyltransferase (TdT) for visualization with fluorescein isothiocyanate (FITC)–conjugated monoclonal antibody to BrdU (FITC–anti-BrdU) 30, 90, or 300 min later (*10*–*12*). Under the conditions used, TdT does not label single-strand DNA nicks (*12*). Nuclei observed 30 min after irradiation displayed a strong FITC signal in parallel stripes corresponding to BrdU incorporation at DNA ends (Fig. 2A). Each pair of unirradiated-irradiated stripes is 3.2 μm wide (1.85 μm unirradiated plus 1.35 μm irradiated). Hence, most nuclei (average diameter 15 to 20 μm) contained six or seven FITC-staining stripes (Fig. 2, A and B). Confocal microscopy demonstrated that parallel stripes of BrdU incorporation were uniform through-

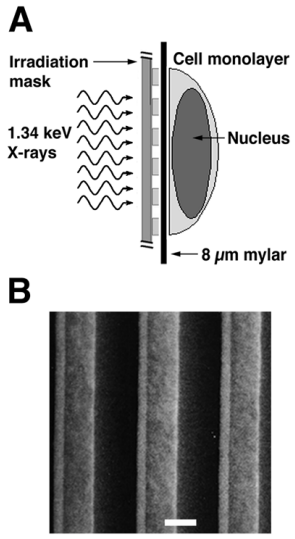

Fig. 1. (**A**) Diagram of the partial volume irradiation scheme (*7*). Thickness of the Mylar surface (8 μm) is not drawn to scale. (**B**) Scanning electron micrograph of irradiation mask. Bar, 1 μm.

B. E. Nelms, Laboratory of Genetics and Department of Medical Physics, University of Wisconsin Medical School, Madison, WI 53706, USA.
R. S. Maser and J. H. J. Petrini, Laboratory of Genetics, University of Wisconsin Medical School, Madison, WI 53706, USA.
J. F. MacKay and M. G. Lagally, Department of Materials Science and Engineering, University of Wisconsin, Madison, WI 53706, USA.

*These authors contributed equally to this work. Names are listed in random order.
†To whom correspondence should be addressed. E-mail: jpetrini@facstaff.wisc.edu